Thin Film Compressive Stresses due to Adatom Insertion into Grain Boundaries

Chun-Wei Pao,[1] Stephen M. Foiles,[2] Edmund B. Webb III,[2] David J. Srolovitz,[1,3] and Jerrold A. Floro[4]
[1]*Department of Mechanical and Aerospace Engineering, Princeton University, Princeton, New Jersey 08544, USA*
[2]*Sandia National Laboratories, Albuquerque, New Mexico 87159, USA*
[3]*Department of Physics, Yeshiva University, New York, New York 10033, USA*
[4]*Department of Material Science and Engineering, University of Virginia, Charlottesville, Virginia 22904, USA*
(Received 23 April 2007; published 19 July 2007)

Atomic simulations of the growth of polycrystalline Ni demonstrate that deposited atoms incorporate into the film at boundaries, resulting in compressive stress generation. Incorporated atoms can also leave the boundaries and thus relieve compressive stress. This leads to a complex interplay between growth stress, adatom incorporation, and surface structure. A simple, theoretical model that accounts for grain size effects is proposed and is in good agreement with simulation results.

DOI: 10.1103/PhysRevLett.99.036102 PACS numbers: 68.60.Bs, 68.55.−a, 81.15.Aa

Volmer-Weber (VW) mode film growth exhibits three stages: at early time, isolated islands nucleate and grow; at intermediate time, adjacent islands coalesce and resultant channels are filled in; and at late time, a continuous film forms and thickens with subsequent growth. *In situ* stress measurements for VW growth demonstrate a complex relation between growth morphology and film stress. For high surface mobility materials, the three growth stages are associated with compressive, tensile, and compressive stress evolution, respectively. Low mobility materials do not show a change back to compression at late times but continue to evolve significant tensile stress after a continuous film has formed [1]. Mechanisms advanced to explain stress evolution during the late time VW growth stage must also account for experiments where, upon interrupting growth, significant tensile stress evolution is observed in high mobility materials and, when growth is resumed, the system rapidly returns to the compressive stress state observed prior to interrupt. Low mobility materials do not show this behavior and, instead, display significantly less tensile stress evolution during growth interrupt [2,3].

Developing a model that explains all experimental observations has not been possible; nonetheless, promising candidates have been advanced. One such model proposes that adatoms reversibly move in and out of grain boundaries (GBs) and, as such, account for both late stage compressive stress evolution (atoms entering GBs) and tensile evolution upon growth interrupt (exiting GBs) [3,4]. The proposed driving force for an atom to enter a GB during deposition is associated with the high chemical potential of an atom on the surface. However, the model, as proposed, depends upon GB diffusion to account for stress relaxation during growth interrupts, and it has been asserted that the corresponding kinetics would be too slow to account for the experimental observations [4]. An adaptation of this model has been advanced that addresses adatom insertion at GBs in the absence of GB diffusivity [5]. Still, other challenges have been made to adatom insertion as the stress evolution mechanism; these models instead invoke surface defect evolution [6,7] or locked-in capillarity stress and recrystallization [8] as alternate mechanisms. However, surface defects have little effect on compressive stresses [9], and the locked-in capillarity stress model cannot explain the tensile relaxation during growth interrupt [8]. Thus, the grain boundary insertion mechanism continues to be called upon to explain experimental data on compressive stress evolution in film growth [10].

In this Letter, we employ molecular dynamics (MD) simulations of Ni deposition onto a Ni(111) surface intersected by two GBs to investigate the interplay of growth stress, grain boundaries, and diffusion. Figure 1 shows the atomistic configuration of the system at 3 times. The simulations employed fixed length periodic boundary conditions in x and y and GB planes are nominally normal to the x direction. The grain boundaries are $\Sigma 79$ [111] symmetric tilt boundaries with misorientation $\theta = 33.99°$. Ni is described via an embedded atom method interatomic potential [11,12]. Deposition is modeled by introducing adatoms at random locations in the xy plane, ~0.5 nm above the free surface so that adatoms are attracted to the surface. The simulations were performed at a constant temperature of $T = 0.5T_m$ (782.5 K) via velocity rescaling of the atoms below the surface. After an atom is deposited, the simulation is run for a relaxation period τ before the next deposition event. Three simulations are performed, labeled systems A, B, and C: A, grain size $L = 5.5$ nm and $\tau = 25$ ps; B, $L = 11$ nm and $\tau = 50$ ps; , and C, $L = 11$ nm and $\tau = 12$ ps. Note that systems A and C have nearly the same deposition rate. The simulation box dimensions in x, y, and z are $2L$, 3.9 nm, and 18 nm, respectively. For system A, the total deposited film thickness $t_f = 3$ monolayers (ML) while for systems B and C, $t_f = 2$ ML.

Figure 1 shows the configuration of the system for $L = 5.5$ nm (system A); atoms are shaded according to their centrosymmetry parameter, which, as a measure of neighbor surroundings, distinguishes between "bulk," surface, and GB atoms. The growth mode is layer-by-layer due to

 © 2007 The American Physical Society

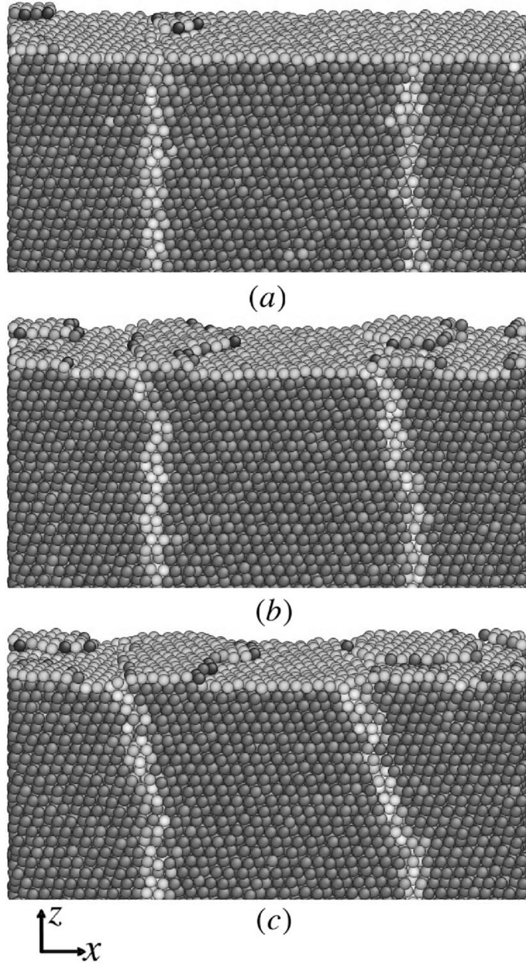

FIG. 1. Simulation snapshots during deposition on the $L = 5$ nm system (system A). Light gray atoms highlight GBs and free surface. (a) $t_f = 0.14$ ML; (b) $t_f = 0.36$ ML; (c) $t_f = 0.49$ ML. Only part of the system is shown in z.

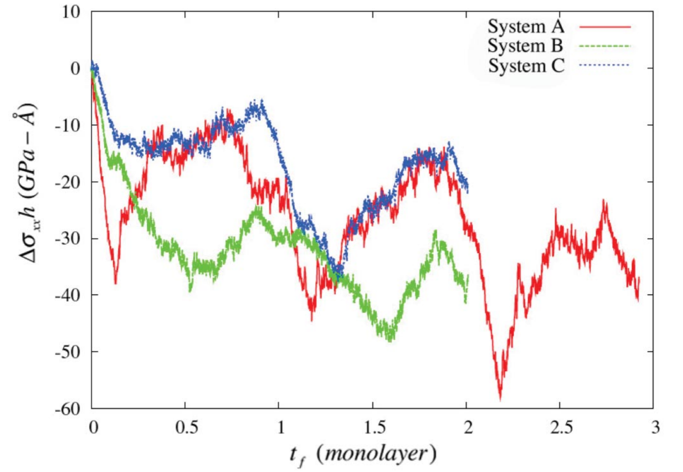

FIG. 2 (color). Stress evolution during deposition for (a) system A, (b) system B, and (c) system C.

the elevated T of the system. This differs from experiments performed at room T; for those, step density is typically much higher and the growth surface is "wedding cake"–like [13]. Simulations were performed at high T to combat temporal constraints in MD (i.e., to enhance atomic diffusion).

In order to measure stress evolution during film growth, we employ a method which is equivalent to measuring substrate curvature change (as done in experiment). That is, we measure changes in the stress-thickness product $\Delta\sigma_{xx}h$, as described in detail in [14]. Change in $\sigma_{xx}h$ is reported, rather than an absolute value, since deposition is modeled on an already continuous film rather than a clean substrate surface. Figure 2 shows $\Delta\sigma_{xx}h$ versus t_f. In all cases, we observe compressive stress evolution, consistent with experimental observations for high mobility materials in late stage VW growth. While oscillations are observed in the simulation data, they are not in experiment—presumably because the experiments inherently average over many grains. The period of the oscillations is $\sim$1 ML—this may be related to the layer-by-layer growth mode. The incremental film stress was calculated (the derivative of the $\sigma_{xx}h$ curve) $\sigma_{xx}^{\rm inc}$, which is approximated by $\sigma_{xx}^{\rm inc} \approx [\Delta\sigma_{xx}h(t_f = 2.0\,{\rm ML}) - \Delta\sigma_{xx}h(t_f = 1.0\,{\rm ML})]/\Delta t_f$. Incremental stresses were $\sigma_{xx}^{\rm inc} \approx -3.14$, ≈ -3.23, and ≈ -3.11 GPa for systems A–C, respectively. Decreasing deposition rate yields larger compressive stresses (cf. systems B and C), consistent with experiment [3,10]. $\sigma_{xx}^{\rm inc}$ in the present study (~ -3 GPa) are larger than observed in experiments ($\lesssim -1$ GPa)—see below.

Figure 3(a) shows the number of atoms per layer (of thickness equal to the 111 plane spacing), N_L as a function of distance from the surface, D ($D = 0$ is the free surface), for system B at three values of t_f. These results demonstrate that during deposition, the atomic density in the film, near the surface, increases; i.e., extra atoms are incorporated into the bulk of the film, near the surface. By monitoring atomic centrosymmetry we confirm that no self-interstitials exist away from the GBs; rather, extra atoms reside at the GBs. The number of extra atoms $N_X(t_f) = \Sigma_D[N_L(D, t_f) - N_0]$ versus t_f is shown in Fig. 3(b), where $N_0 = N_L(D = \infty)$. The extra atoms penetrate into the film to a depth of at least 20 Å. Adatom trapping in interstitial-like sites near step edges has been proposed as a compressive stress generation mechanism [15] and recent experiments and calculations confirmed related behavior on Au film surfaces [16]. This is not observed in these simulations, which is likely related to the low step density on our near-ideal planar surface. Examination of Figs. 3(a) and 3(b) shows that the number of extra atoms first increases during deposition and then decreases. This means that some of the extra, incorporated atoms move out of the GB and back onto the free surface. In fact, N_X is oscillatory, with a period of $\sim$1 ML, as for the stress-thickness product. This strongly suggests that $\sigma_{xx}h$ correlates with N_X. These results show that adatom incorporation into GBs and their egress from GBs occurs very rapidly and is responsible for increases and decreases in the compressive film stress, respectively, during deposition.

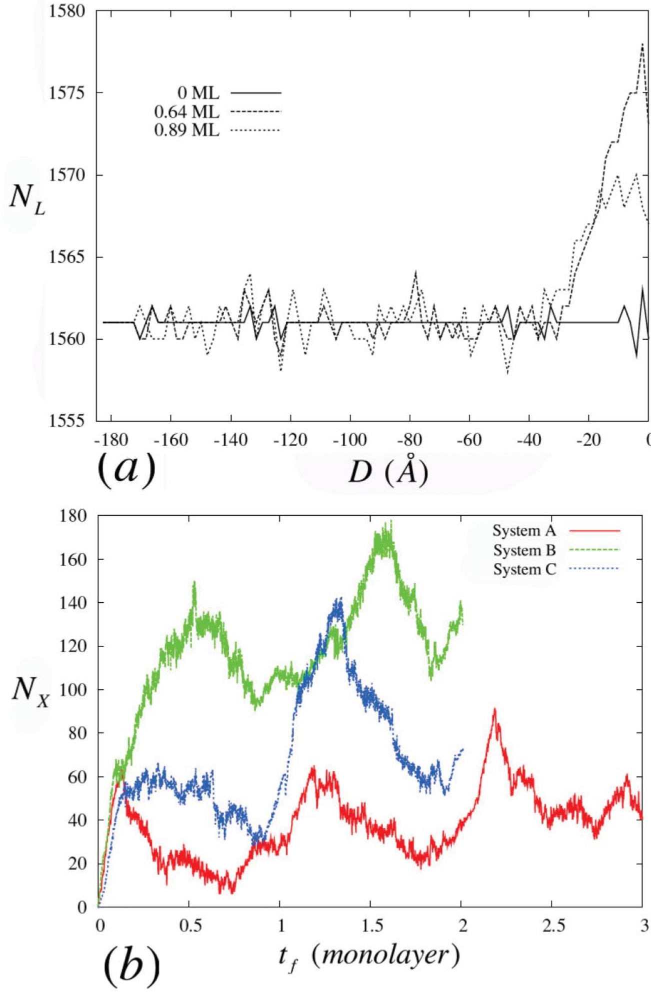

FIG. 3 (color). (a) Number of atoms in the film bulk N_L vs depth from the surface D for system B at $t_f = 0$, 0.64, and 0.89 ML. (b) The number of extra atoms N_X incorporated into the grain boundaries vs film thickness t_f.

The grain boundary insertion model [3,4] invokes a chemical potential difference $\Delta\mu$ between the growth surface and GB, $\Delta\mu = \Delta\mu_0 + \delta\mu_s + \sigma\Omega$. $\Delta\mu_0$ is the difference between the free surface and GB chemical potentials in the absence of growth, $\delta\mu_s$ is the increase in surface chemical potential associated with the deposition flux, and $\sigma\Omega$ represents the elastic work done by inserting an atom of volume Ω into the grain boundary in the presence of a normal stress σ across the GB. We can interpret our results in terms of this model. The first term is dominated by the difference in the formation energy of an adatom on the surface versus a self-interstitial in the grain boundary. For the polycrystalline film considered here, we find that this difference is in excess of 0.5 eV/atom (surface ~1.5 eV, GB <1 eV). Slower deposition rates give atoms more time to diffuse into the GB before they are buried by the next layer of atoms. This is consistent with our simulation results shown in Fig. 3(b). One of the unique features of the present work is the observation that the number of extra atoms in the grain boundary increases and decreases with a period that is similar to the time to deposit a single monolayer. At the beginning of the deposition of each monolayer, adatoms are either isolated or in small clusters, and hence have very high energies. As the monolayer fills, the average cluster size increases and the energy per adatom drops. Hence, the chemical potential of the surface drops and adatoms that were in the grain boundary start to come back out. This explains the observed cyclic nature of the stress and N_X. We note, that unlike other models, this approach does not require any assumptions about tensile surface stresses, island coalescence, etc. [4] and is consistent with the standard understanding of how surfaces evolve during growth.

Figure 3(b) shows that N_X is smaller for system A than for either systems B or C. This is simply a result of the fact that the strain energy per extra atom is larger in a small system than a large one because strain due to adatom incorporation is larger for smaller grain size in system A. This can be understood in terms of a stress analysis akin to that performed in [3]. The film stress due to adatom incorporation can be written approximately as

$$\Delta\sigma_{xx} \approx \frac{-E(a-d)}{L+d} N_X \left(\frac{\pi(a/2)^2}{2L_y h}\right) = -\frac{\pi E a^3}{8LL_y h}\left(1-\frac{d}{a}\right)N_X, \quad (1)$$

where E is the film elastic modulus, L is the grain size, L_y is the simulation cell size in y, a is the atomic diameter, h is the thickness of the film, and d is the GB "width" in x (i.e., the gap between neighboring grains). d can be related to the GB free volume v by $v = dL_y h$ and thus depends on the GB type; its value is typically less than an atomic diameter. The term $-E(a-d)/(L+d)$ refers to the compressive stress acting on the grain if the GB with width d is completely filled with inserted atoms with diameter a. Note that the expression for stress in [3] is the special case with $d = 0$, which may lead to overestimation of stress because there is always free volume associated with GBs. The term $N_X\pi(a/2)^2/2L_y h$ is the fraction of the boundary area occupied by N_X inserted atoms (the factor of 2 accounts for the two GBs in our system). Assuming that $d \ll L$, we can rewrite the stress-thickness product as

$$\Delta\sigma_{xx}h \approx -\frac{\pi E a^3(1-\frac{d}{a})}{4L_x L_y} N_X = -\frac{\pi E a^3 \rho_X}{4}\left(1-\frac{d}{a}\right), \quad (2)$$

where $2L \approx L_x$ and $\rho_X = N_X/L_x L_y$ is the density of extra atoms per unit film surface area. This demonstrates that $\sigma_{xx}h$ should be a linear function of ρ_X with slope $-(\pi/4)Ea^3(1-d/a)$ regardless of grain size and deposition rate. The geometric parameter α in [3] is manifested in our model as $(\pi/4)(1-d/a)$.

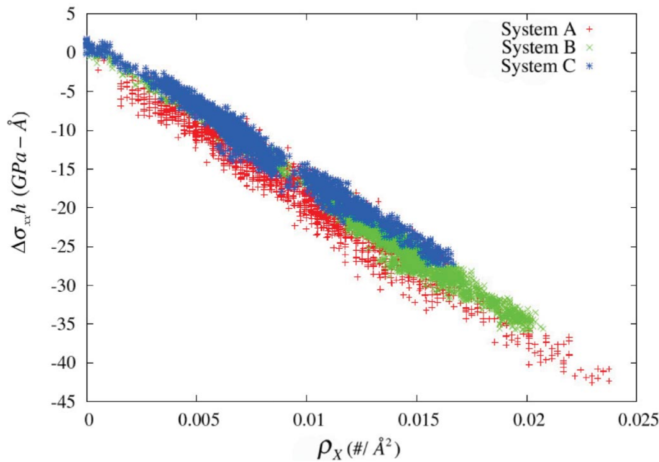

FIG. 4 (color). The film stress-thickness product $\Delta\sigma_{xx}h$ vs the density of incorporated extra atoms ρ_X for three deposition simulations.

The stress-thickness product is plotted versus ρ_X in Fig. 4. All data collapse onto a single line, consistent with our prediction. The fitted slope in Fig. 4 is -1820 GPa Å^3. In our simulations, $E = 191.6$ GPa and $a = 2.51$ Å and the GB free volume is estimated from the difference in volume of a cell with the GB and bulk crystal with the same number of atoms, i.e., $d = 0.31$ Å. Substituting these data into Eq. (2) yields a slope of -2099 GPa Å^3. The fitted slope is 87% of that of the theoretical prediction and therefore is in very good agreement (considering the simplicity of the stress approximation). This demonstrates that adatom incorporation and, specifically, ρ_X is an important factor for predicting the stress-thickness (wafer curvature) during polycrystalline thin film growth.

Despite the success, we note that the magnitude of the compressive stress found in the simulations is significantly greater than in experiments. Since it is generally accepted (and observed in our simulations) that *lower* deposition rates *increase* compressive stresses, this is clearly not an artifact of the high deposition rates employed in the simulations. Our simulations were also performed at a temperature that is much higher than in most growth experiments; this greatly enhances atomic mobility and the likelihood of adatoms reaching a GB. Atomic mobility is further enhanced by the extreme planarity (low step densities) of the surfaces in our simulations, relative to the much higher step density surfaces seen experimentally during low temperature growth. Steps are effective adatom traps. We suspect that it is the enhanced atomic transport on the surface that is responsible for the larger growth stresses observed in simulation as compared with experiment.

Figure 3(a) shows incorporated atoms penetrate ~20 Å after $t_f = 0.64$ ML, corresponding to simulation time ~45 ns. While T in simulations is high, adatom advancement along the GB is remarkably rapid. Mishin *et al.* [17,18] has shown that self-interstitial diffusion rates in GBs in Cu over a very wide range of T. Earlier literature (e.g., [4]) suggested that GB diffusion kinetics may not be sufficiently fast to account for the rapid compressive stress relief upon interrupting growth. However, data in [17–19] along with the present results demonstrate that GB incorporation and diffusion are quite fast and may explain late stage VW stress evolution for many material systems. Since atoms can readily exit GBs when the surface structure evolves fast transport can explain both the abrupt change in surface stress during growth interrupt and the periodic nature of the growth stress during deposition. This provides a link between surface structure (e.g., see [7]), surface chemical potential, and growth stress.

In summary, MD simulations show adatoms incorporate into GBs and this process directly correlates with compressive stress evolution. A theoretical model suggests the density of atoms incorporated ρ_X is linearly proportional to stress-thickness product, regardless of grain size and deposition rate; simulations support this conclusion. By refining interpretations in [3], a direct connection between GB free volume, surface structure, and the stress evolution during film growth is provided.

[1] R. Aberman and R. Koch, Thin Solid Films **129**, 71 (1985); R. Aberman, Vacuum **41**, 1279 (1990).
[2] A.L. Shull and F. Spaepen, J. Appl. Phys. **80**, 6243 (1996).
[3] E. Chason, B.W. Sheldon, L.B. Freund, J.A. Floro, and S.J. Hearne, Phys. Rev. Lett. **88**, 156103 (2002).
[4] P.R. Guduru, E. Chason, and L.B. Freund, J. Mech. Phys. Solids **51**, 2127 (2003).
[5] B.W. Sheldon, A. Ditkowski, R. Beresford, E. Chason, and J. Rankin, J. Appl. Phys. **94**, 948 (2003).
[6] C. Friesen and C.V. Thompson, Phys. Rev. Lett. **89**, 126103 (2002).
[7] C. Friesen, S.C. Seel, and C.V. Thompson, J. Appl. Phys. **95**, 1011 (2004).
[8] R. Koch, D. Hu, and A.K. Das, Phys. Rev. Lett. **94**, 146101 (2005).
[9] C. Pao, D.J. Srolovitz, and C.V. Thompson, Phys. Rev. B **74**, 155437 (2006).
[10] A. Bhandari, S.J. Hearne, and B.W. Sheldon, J. Appl. Phys. **101**, 033528 (2007).
[11] S.M. Foiles and J.J. Hoyt, Acta Mater. **54**, 3351 (2006).
[12] M.S. Daw, S.M. Foiles, and M.I. Baskes, Mater. Sci. Rep. **9**, 251 (1993).
[13] M.J. Rost, D.A. Quist, and J.W.M. Frenken, Phys. Rev. Lett. **91**, 026101 (2003).
[14] C. Pao and D.J. Srolovitz, Phys. Rev. Lett. **96**, 186103 (2006).
[15] F. Spaepen, Acta Mater. **48**, 31 (2000).
[16] H.W. Zandbergen, C. Pao, and D.J. Srolovitz, Phys. Rev. Lett. **98**, 036103 (2007).
[17] M.R. Sørensen, Y. Mishin, and A.F. Voter, Phys. Rev. B **62**, 3658 (2000).
[18] A. Suzuki and Y. Mishin, Interface Sci. **11**, 131 (2003).
[19] A. Suzuki and Y. Mishin, Interface Sci. **11**, 425 (2003).